Non-Engine Order Blade Vibration in a High Pressure Compressor

by

M. Baumgartner, F. Kameier, J. Hourmouziadis*)

BMW Rolls-Royce AeroEngines,
Eschenweg, 15827 Dahlewitz, Germany

**) Technical University Berlin,*
Luftfahrtantriebe, Institut für Luft- und Raumfahrt,
Marchstraße 14, 10587 Berlin, Germany

Abstract

High amplitude levels of blade vibration have occurred on the first rotor of a multi stage high pressure compressor. The frequencies are not in resonance with harmonics of the rotor speed. The excitation is aerodynamically caused and associated with a rotating flow instability in the blade tip region of the first compressor stage. A vortex shedding mechanism can be interpreted as a rotating source to generate pressure waves. The source moves relative to the blade row at a fraction of the rotor speed, similar to the 'well known mechanism' of rotating stall.

To investigate the unsteady flow field in the tip region of the rotor and its relation to the blade vibration, measurements of the pressure and velocity fluctuations in the vicinity of the blade tips are compared with blade vibrations. A calculation model of the spectral characteristics of the pressure fluctuations confirms the measured data. The effect is sensitive to aerodynamic blade loading so that a modification in the design could reduce the mechanism of the rotating excitation.

1. Introduction

A major task in the development programme of a multistage compressor is to ensure that the blades have no severe vibration problem. This definition depends upon the stress criteria, which are linked to the fatigue properties of the component. Although in the design phase much effort is being undertaken to produce blades with a satisfactory mechanical integrity it is limited by the fact that the excitation forces are difficult to predict. Usually the design work concentrates on the calculation of frequencies and the stress distributions associated with particular mode-shapes. The standard procedure is to generate a Campbell-diagram, where the frequencies for different running conditions are plotted versus rotor speed. The intercepts of engine order spokes with the frequency lines give the information required to make a decision whether the particular design is acceptable or not. The final assessment of the complete dynamic picture, however, is taken from engine test runs.
With the knowledge of the predicted frequencies the vibration modes are able to be identified from the measured frequencies. The most important job is to determine whether the magnitude of the highest vibration levels is below the admissible limits set. Normally the highest amplitudes occur when an engine harmonic coincides with an eigenfrequency of the blade. In this case the blades are being excited by unsteady aerodynamic forces caused by a non-uniform pressure field due to wakes of upstream vanes, potential effects of downstream vanes or further unsymmetrical flow conditions.

Sometimes, however, high vibration amplitudes cannot be attributed to engine orders. This requires a careful examination because the vibration might be associated with stall or acoustic resonance in the duct.

In this paper an experimental investigation about the aerodynamic sources which lead to high non-engine order vibration on the first stage of a multi-stage high pressure compressor are presented. The unsteady pressure and velocity fluctuations are determined by pressure transducers mounted at the casing wall just upstream of the first rotor and by a hot-film probe at the trailing edge region of the blade adjustable in the radial direction. The blade response is measured by strain gauges fitted on the aerofoil.

2. Classification and Evaluation of Flow-Induced Vibrations

Amongst other tasks the prediction of frequencies and mode-shapes is a standard procedure when designing compressor blades. A Campbell-diagram in combination with design criteria is a powerful tool to get a clear picture of the dynamic behaviour of the blade. The intercepts of frequency and engine order lines tell at what engine speed the forced vibration is about to occur. The aerodynamic excitation and the mechanical

damping properties that affect the resonance-amplitudes are not covered.

Self exciting mechanism like flutter, acoustic pressure waves or rotating instabilities, however, do not even allow to predict the onset of high amplitudes. Often they occur in an experimental engine-test programme when the stability boundaries of the compressor are being determined.

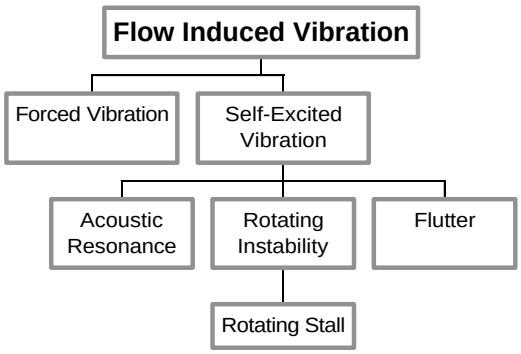

Figure 1: Classification of flow-induced vibration

2.1 Forced Vibration

The blades rotate through a steady flow field that is non-uniform in circumferential direction. This flow field is being experienced by the blades as cyclic pressure fluctuations varying in time. Strain gauges fixed to cantilevered blades will observe the response of the blades as a series of sinusoidal excitations according to a Fourier-decomposition of the excitation signal. Resonance occurs in the case of an eigenfrequency of the blade coinciding with any of these harmonics, which is an integer multiple of the rotational speed.

The dynamic behaviour of the coupled blades is different compared to cantilevered blades (Thomas 1956). The whole bladed disk assembly forms complex vibration modes. Every classical mode like 1st flap (1F), 1st torsion (1T) is, as it were, an upper term for a complete family of individual modes, which are classified as nodal diameters (ND). The maximum number of nodal diameters is usually half of the number of blades (N) per stage. Whereas the blades perform an in-phase vibration mode for a zero ND, they vibrate out-of-phase for a N/2 ND (Ewins 1987).

Since for tuned cyclic systems every mode appears in pairs with orthogonal mode-shapes resonance conditions are only possible if the excitation forces are orthogonal as well. As a result of this a backward travelling wave builds up. This is the most significant difference to a cantilevered blade resonance condition:

A forced vibration resonance is only possible if the integer multiple of the rotor speed (Engine Order EO)

has the same integer value as the nodal diameter (ND).

The pressure distribution in the circumferential direction can be regarded as a series of sinusoidal waves for any frequency. So the excitation frequency of say a 5th EO also contains, besides the wave with 5 lobes, also waves with 3,4,6 etc. lobes. Thus an aerodynamic wave with 6 lobes having the frequency, which is exactly the 5th EO, may excite the 6thND structural bladed disc mode if the frequencies fit.

This may not count for the standard forced response case where the 5th aerodynamic ND is the strongest for a 5th EO. However the aerodynamic ND has to coincide with the structural ND and not the EO. Therefore at a non-engine-order resonance condition the aerodynamic and structural ND are the same.

For rotors with coupled blades it is necessary to distinguish between strict periodic excitation and periodic excitation. Strict periodic excitation only yields to integer multiples of the first harmonic wave lobe-number. Periodic excitation with small disturbances of the pressure field results to various waves having all possible aerodynamic ND.

2.2 Self-Excited Vibration

In contrast to forced vibration the alternating force disappears when the vibration stops. The alternating force is controlled by the motion.

2.2.1 Acoustic Resonance

Acoustic pressure fluctuations with a propagation speed being the speed of sound can cause high level vibrations of mechanical structures. There is only one frequency of an acoustical resonance and its wave length has to fit with a geometrical length to generate high pressure levels. Bleed cavities in turbomachines have this kind of resonance.

The frequency depends only on the geometry and not on the flow velocity. Similar to the sound radiation of a Helmholtz-Resonator the frequency is influenced by the resonator volume, the speed of sound and the diameter of the neck or the hole in the resonator body (Fletcher and Rossing 1991). The excitation is a function of the vortex shedding frequency, which is caused by the tangential flow across the inlet hole.

Parker and Stoneman (1985) also conclude that the source of an acoustic resonance excitation in turbomachines is due to vortex shedding from the rotor or stator blades or even from support struts.

Vortex shedding, however, does not necessarily need to excite an acoustic field. Particularly in the immediate vicinity of the blade pressure fluctuations can be generated the propagation speed of which differs from the speed of sound.

2.2.2 Rotating Flow Instabilities

The best known rotating flow instability in turbomachines is rotating stall. The increasing of the incidence angle of a stage leads to a boundary separation which due to flow non-uniformities sets on at one or more circumferential positions. A stalled blade results in a flow diversion that tends to overload one adjacent blade and to unload the other adjacent blade. This causes the overloaded blade to stall and to unload the originally stalled blade, thus generating the stall cell to move around the blade row with a smaller velocity, which is about half of the rotor speed. (Greitzer 1980). Pressure transducer can measure that pattern leading to a discrete frequency with harmonics of it.

Rotating stall can be regarded as a special case of a rotating aerodynamic instability reported by Kameier (1994) and Kameier and Neise (1995/II). The combination of flow recirculation due to an enlarged tip clearance and a boundary separation causes a vortex shedding in the tip region of the rotor blades which leads to high pressure fluctuations and might cause high level blade vibration. Unlike the rotating stall the pressure fluctuations are unsteady in a frame rotating with this instability pattern. Fig. 2 illustrates this effect. An observer moving with the instability cell would measure a discrete frequency signal associated with the pressure fluctuation whereas moving with the rotating stall cell he would not detect any signal due to the stall. In a non-rotating coordinate system the rotating instability would be measured as a range of frequencies with a characteristic frequency signature different to the rotating stall which would be received as a single discrete frequency with possible harmonics of it at the most.

One can imagine rotating instability as a rotating loudspeaker that is moving relative to the rotor blade in the circumferential direction.

2.2.3 Flutter

A number of investigations and explanations about flutter have been published about the different kind of flutter and excitation mechanism. Flutter is a flow induced instability at or close to the eigenfrequency of the rotor blade. The frequencies of flutter are not an integer multiple of the engine speed. Because even small stochastic vibration levels are sufficient to build up high amplitudes no periodic external excitation source is required. The input-energy from the fluid motion to the blade is higher than the dissipation-energy provided by the mechanical damping.

Whereas it is possible to accelerate or decelerate through the speed range of an engine order vibration, the flutter amplitudes can only be reduced by backing off in speed.

A literature survey shows that plenty of papers are being published every year. A detailed overview about various aspects in flutter and a classification is given by Fung (1955) and Sisto (1987).

3. Theoretical Formulation of the Rotating Source Mechanism

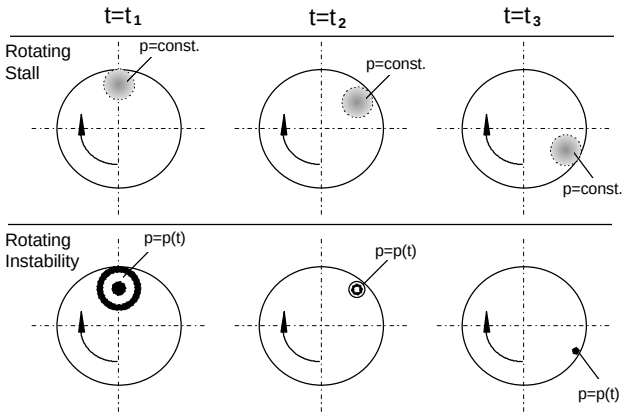

Figure 2: Schematic presentation of rotating stall and rotating instability pressure variation at different times

In a fixed frame of reference a one dimensional description of the unsteady azimuthal pressure fluctuation in an annulus $p(\varphi^F,t)$ can be thought as a series of sinusoidal waves with different lobes α across the circumference having time-dependent amplitudes A and phase angles Φ. Since the time-dependent values can be expressed as continuous spectra, the pressure fluctuation follows as (Tyler and Sofrin 1962)

$$p\left(\varphi^F, t\right) = \sum_{n=1}^{\infty} \sum_{\alpha=-\infty}^{+\infty} A_{n\alpha}^F \cos\left(\alpha\varphi^F - \omega_n^F t - \Phi_{n\alpha}^F\right) \qquad (1)$$

where the amplitudes are schematically illustrated in Fig. 3.

If at a certain off-design engine operational point a periodically occurring boundary separation causes a von-Kármán type of vortex street then the vortices can

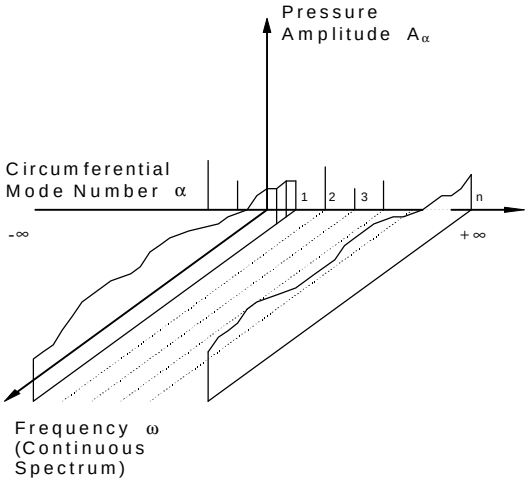

Figure 3: Schematic of circumferential Fourier decomposition.

be interpreted as a rotating sound source mechanism of the frequency ω_{SM}^{S} exciting all sort of aerodynamic nodal diameter patterns $(-\infty < \alpha < +\infty)$ with that frequency. Assuming the source is rotating relative to the rotor with an angular velocity of Ω_S^F then in a frame of reference rotating with the source (S) the pressure distribution can be given in the same way as in equation (1).

$$p\left(\varphi^S, t\right) = \sum_{n=1}^{\infty} \sum_{\alpha=-\infty}^{+\infty} A_{n\alpha}^{S} \cos\left(\alpha\varphi^S - \omega_n^S t - \Phi_{n\alpha}^S\right) \quad (2)$$

Similar in a coordinate system fixed with the rotor

$$p\left(\varphi^R, t\right) = \sum_{n=1}^{\infty} \sum_{\alpha=-\infty}^{+\infty} A_{n\alpha}^{R} \cos\left(\alpha\varphi^R - \omega_n^R t - \Phi_{n\alpha}^R\right) \quad (3)$$

The transformation of the frequencies from the source frame to the fixed frame (F) and to the rotating frame of reference (R) follows with the geometric relations given in Fig. 4.

$$\varphi^F = \varphi^S + \Omega_S^F \, t \quad , \qquad (4)$$

$$\varphi^F = \varphi^R + \Omega_R^F t \quad , \qquad (5)$$

$$\varphi^S = \varphi^R + \Omega_R^S \, t \quad , \qquad (6)$$

$$\Omega_R^F = \Omega_S^F + \Omega_R^S \quad . \qquad (7)$$

In equation (4) the angular coordinate in the fixed frame of reference φ^F is the sum of the angular coordinate in the source frame of reference φ^S and the angular distance of the source frame of reference relative to the fixed frame of reference Ω_S^F.

Because the rotating source will be seen from the rotor system, the equations (6) and (7) can be modified with the relation

$$\Omega_R^S = -\Omega_S^R \qquad (8)$$

to $\varphi^S = \varphi^R - \Omega_S^R \, t$ and (9)

$$\Omega_R^F = \Omega_S^F - \Omega_S^R \quad . \qquad (10)$$

Substituting equation (4) into (2)

$$p\left(\varphi^F, t\right) = \sum_{n=1}^{\infty} \sum_{\alpha=-\infty}^{+\infty} A_{n\alpha}^{F} \cos\left(\alpha\varphi^F - \left(\omega_n^S + \alpha\Omega_S^F\right)t - \Phi_{n\alpha}^F\right) \qquad (11)$$

allows to determine the frequencies of the rotating source frame in the fixed frame by comparing (11) with (1). For the aerodynamic modes vibrating with the source frequency ω_{SM}^S the following relation can be given

$$\omega_{SM}^F = \omega_{SM}^S + \alpha \, \Omega_S^F \quad . \qquad (12)$$

In the same way the substitution of equation (9) into (2) results in a formulation of the rotating source frequency ω_{SM}^R in the rotating system

$$\omega_{SM}^R = \omega_{SM}^S + \alpha \, \Omega_S^R \quad . \qquad (13)$$

Note that the α-values might be positive and negative according to the equations (1),(2) and (3).

Equations (12), (13) and (10) result in an expression for the aerodynamic nodal diameters

$$\alpha = \frac{\omega_{SM}^F - \omega_{SM}^R}{\Omega_R^F} \quad . \qquad (14)$$

(14) and (12) allow the frequency of the pressure wave in source system to be calculated:

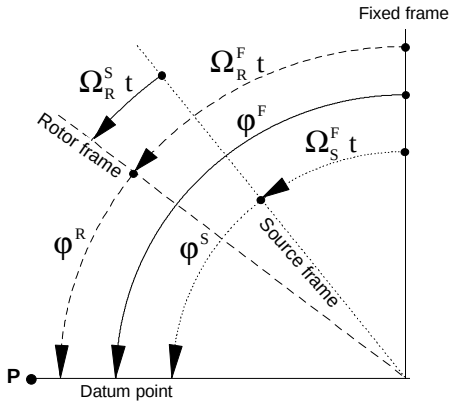

Figure 4: Rotational direction of the source frame and the rotor frame relative to the fixed frame of reference.

$$\omega_{SM}^{S} = \omega_{SM}^{F} - \left(\omega_{SM}^{F} - \omega_{SM}^{R}\right)\frac{\Omega_{S}^{F}}{\Omega_{R}^{F}} \qquad (15)$$

For two adjacent α the equations (12) and (13) lead to the angular velocity of the rotating source

$$\Omega_{S}^{F} = \omega_{SM(\alpha+1)}^{F} - \omega_{SM(\alpha)}^{F} \; . \qquad (16)$$

The rotating stall flow pattern does not generate frequency components in the frame of reference which is rotating with the stall. Therefore $\omega_{SM}^{S} = 0$ and from the equations (12) and (13) follow for the fixed and rotating frame of reference

$$\omega_{RS}^{F} = \alpha \;\; \Omega_{RS}^{F} \qquad (17)$$

and

$$\omega_{RS}^{R} = \alpha \;\; \Omega_{RS}^{R} \quad . \qquad (18)$$

A comparison between equations (17) and (18) with equations (12) and (13) shows that the rotating stall is a special case of the rotating instability. Ω_{RS}^{F} and Ω_{RS}^{R} are the angular velocities of the rotating stall cell in the fixed and rotating frame of reference. Since Ω_{RS}^{F} is usually smaller than Ω_{R}^{F} but propagating in the same direction, the sign of Ω_{RS}^{R} is negative. Thus $\omega_{RS}^{F} > 0$ and $\omega_{RS}^{R} < 0$.

The equations (11), (12) and (13) show for a positive source frequency $\omega_{SM}^{S} > 0$ the relationship

$$\omega_{SM}^{F} > 0 \quad \text{for} \quad \alpha > 0 \quad \text{or} \quad -\alpha > -\omega_{SM}^{S} / \Omega_{S}^{F}$$

$$\omega_{SM}^{R} > 0 \quad \text{for} \quad \alpha < 0 \quad \text{or} \quad \alpha < -\omega_{SM}^{S} / \Omega_{S}^{R}$$

According to equation (1) α is always positive and negative, therefore it is necessary to consider that the frequencies can be negative. Because the measurement devices always give positive frequencies equation (14) has to be rewritten to

$$|\alpha| = \frac{\left|\omega_{SM}^{F}\right| \pm \left|\omega_{SM}^{R}\right|}{\left|\Omega_{R}^{F}\right|} \quad . \qquad (19)$$

Fig. 5 explains how the frequencies and aerodynamic nodal diameters relate in the source frame and in the fixed frame. In the source-frame the source-frequency ω_{SM}^{S} can, according to equation (2), excite numerous pressure waves $\left(-\infty < \alpha < +\infty\right)$, whereas the rotating stall would only cause a constant pressure distribution thus having a particular pressure wave with a certain α. The transformation into the fixed frame leads, according to equation (12), to a straight line containing different frequencies for the rotating instability but only to a single frequency for the rotating stall. Because of equation (16) the difference between adjacent peaks is constant, which is a characteristic of rotating instability when interpreting measured pressure data in the fixed-frame, Fig. 5 also shows that any aerodynamic nodal diameter can excite a cantilevered blade mode, whereas a resonance for a bladed disc is only possible if the mechanical and aerodynamical nodal diameters are the same. For $\omega_{SM}^{S} = 0$ and $\Omega_{S}^{F} = 0$ equation (10) and (13) lead to forced response conditions.

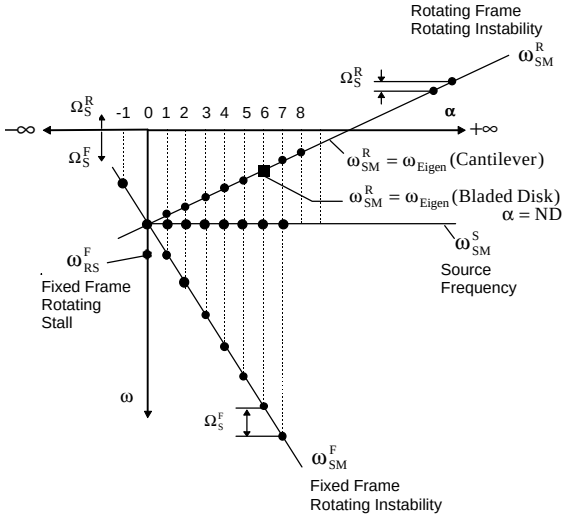

Figure 5: Schematic of frequencies and aerodynamic nodal diameters

4. Blade Design, Test-Rig, Experimental Set-up and Measurement Technique

4.1 Blade Design

Fig. 6 shows the 1T mode-shape of the first rotor blade of a multi-stage high pressure axial compressor. The aerofoil is coupled by means of a snubber with the adjacent blades. This is necessary to avoid a low engine order excitation within the running range because the blade features a high aspect ratio and thin profile thickness design. Strictly speaking the plotted mode-shape is the analytical solution for the 8thND.

The mode-shape for the entire assembly is displayed in Fig. 7.

Figure 6: 1T Modeshape (1 T) of the first rotor blade of a multi-stage high pressure axial compressor

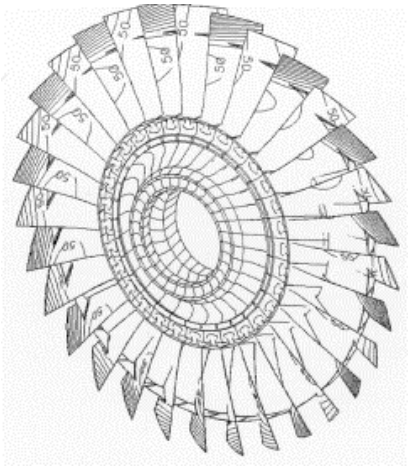

Figure 7: Mode shape for the entire assembly

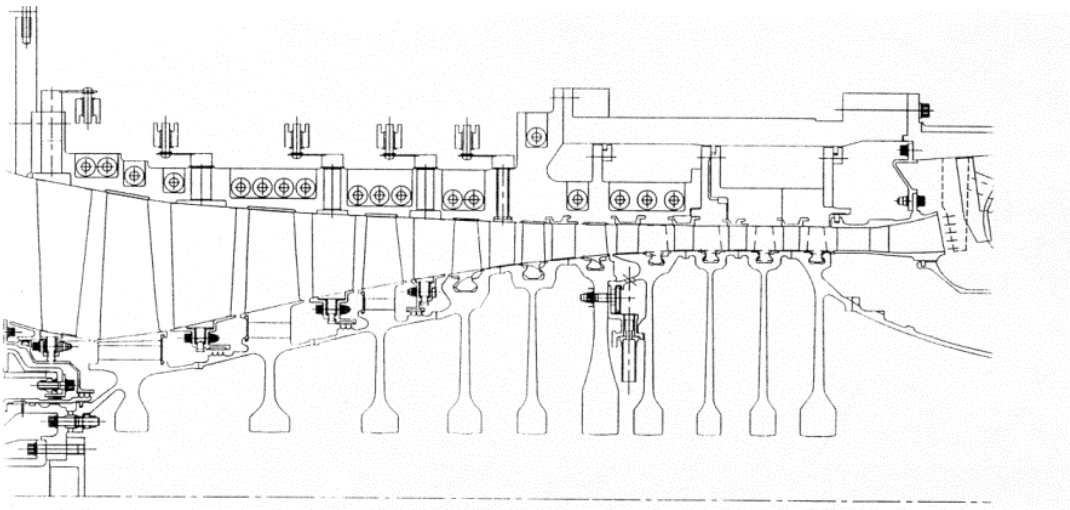

Figure 8: Schematic of the 10 stage high pressure compressure.

4.2 Test-Rig

Fig. 8 gives an outline of the 10 stage high pressure compressor test rig facility that is being driven by a 18 MW electric motor. The test compressor has a pressure ratio of 16.2, which leads to a temperature rise of 400 K. The axial Mach-number is 0.52 at the inlet and 0.25 at the outlet. The first rotor stage has a diameter of 0.52 m with a hub-to-tip ratio of 0.5, the numbers for the last stage are 0.47 m and 0.9. The max. speed is 16000 rpm and the max. mass flow is 35 kg/s. To allow different loading conditions in the front stages the first four variable vane stages are independently adjustable.

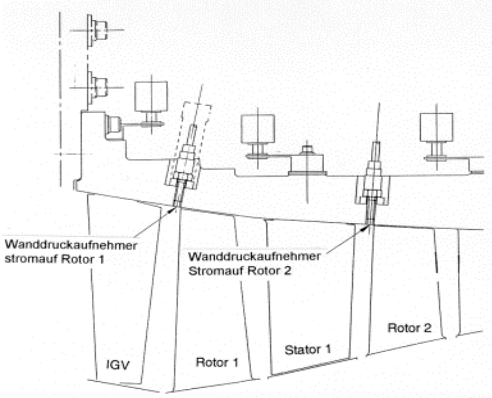

Figure 9: Experimental set-up of the Kulite XTE 190 transducer in the casing wall.

4.3 Experimental Set-up

The pressure fluctuations on the casing wall have been monitored by using Kulite XTE 190 pressure transducers. They are mounted flush with the inner wall, upstream of the blade leading edge of the first stage (Fig. 9).

A single hot-film probe (Dantec 55R03 Fiber-Film-Sensor) has been employed to measure the velocity fluctuations in the blade tip trailing edge region of the first rotor. To vary the radial measurement position the probe is able to be moved radially from the casing.

The stress measurements have been carried out with standard strain gauges measurement technique. The signal is being transmitted through a slip-ring from the rotational system to the fixed system.

4.4 Measurement Technique

The complete transient data information has been recorded on a multi-channel tape recorder. A HP 9000 UNIX workstation has controlled the data acquisition and the processing unit HP 3565 with anti-alias protection, FFT and averaging processor on each channel. A standard multi-channel FFT-Analyser software has been applied for evaluating the recorded data. Several replays from tape allow nearly infinite resolutions in frequency.

To display the frequency signature of a component against engine speed or against time the Z-Mod plots are used. They are similar to waterfall plots except that each spectrum is displayed as a single vertical line with amplitudes being represented by a colour scale (in this paper for copy reasons by a grey scale). For minimising noise effects each plotted spectrum in the Z-mode is an average of 10 measured spectra. The frequency spectra contain 1600 lines with a span of 12.8 kHz that is a frequency resolution of 8 Hz.

5. Test Analysis and Interpretation

5.1 Comparison of Pressure Fluctuations and Blade Vibration

Fig. 10 shows for a slow acceleration the Z-Mod plots versus speed of the pressure transducer in the casing wall (top) and the blade strain gauge (bottom). The upper diagram displays a frequency span of 8.5 kHz for the wall pressure and the lower diagram a frequency span of 3 kHz for the blade vibrations. The blade passing frequency is clearly visible on the Kulite picture as a thick 31st EO line. Between 89.5 - 96.5 % rotor speed high wall pressure fluctuations occur. Also at this speed range high blade vibration amplitudes for the 1F and 1T modes build up the maxima of which do not intersect with the engine order lines. More detailed information of this effect is given by individual spectre plots at engine speed of 85%, 94% and 101% (Figure 11, 12, 13). These pictures illustrate the correspondence of blade vibration and wall pressure fluctuations.

At 85 % speed (Figure 11) the wall pressure spectrum shows harmonics of rotating stall frequencies (equation 22) and the first blade passing frequency (1st BPF). The lowest rotating stall frequency is larger than the rotor shaft speed (1st EO). This presumably results from an asymmetric distribution of two stall cells that cause the 3rd and 4th frequency peaks. The blade passing frequency is being picked up by the pressure transducer because the passing blades generate an oscillating potential pressure field. The levels are obviously more dominant than the pressure field of the rotating stall wave. Thus the stall is more likely to be a part span stall rather than a full span stall, which would have resulted in higher levels due to flow separation along the entire blade. The blade vibration shows low activity for the 1st bending and 1st torsion mode frequencies.

At 94.3 % mechanical speed (Figure 12) high blade vibration amplitudes for the 1F and 1T modes build up. The pressure spectrum shows large fluctuations. The peaks, however, are still smaller than the blade passing frequency. The frequencies are in the range of about half the blade passing frequency. The blade vibration frequencies neither correspond to integer

multiples of the engine speed nor fit to the frequency components of the pressure fluctuations.

For higher compressor speed (Figure 13) the blade vibration amplitude levels fade away. Simultaneously the levels of the pressure fluctuations disappear. Only multiples of the rotor speed with the highest amplitudes for the blade passing frequency are visible.

5.2. Explanation of Pressure Fluctuation Frequencies

In addition to Fig. 12, Fig.14 details the frequency pattern of the pressure field with an increased frequency resolution at about 94% mechanical speed.
This picture shows constant distances between the peak amplitudes. This would confirm equation (16). The distance of the spikes is 155 Hz that is 62% the rotor speed. The measured frequencies behave according to equation (12) or the straight line in the fixed frame of Figure 5.
The results tie up very well with results by Kameier and Neise (1995 I) on a low speed fan, where similar frequency patterns have occurred. (Fig.15).
A more thorough investigation with a rotating loudspeaker confirmed the characteristic of the

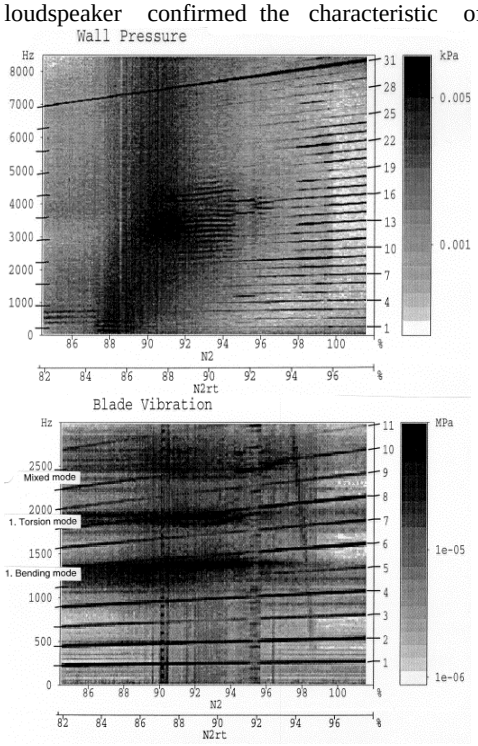

Figure 10: Comparison of blade vibrations and wall pressure fluctuations.

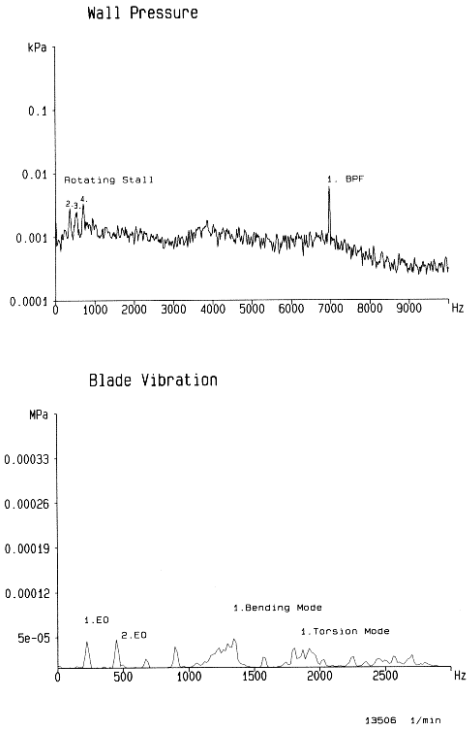

Figure 11: Comparison of wall pressure and blade vibration spectra, N=85 %.

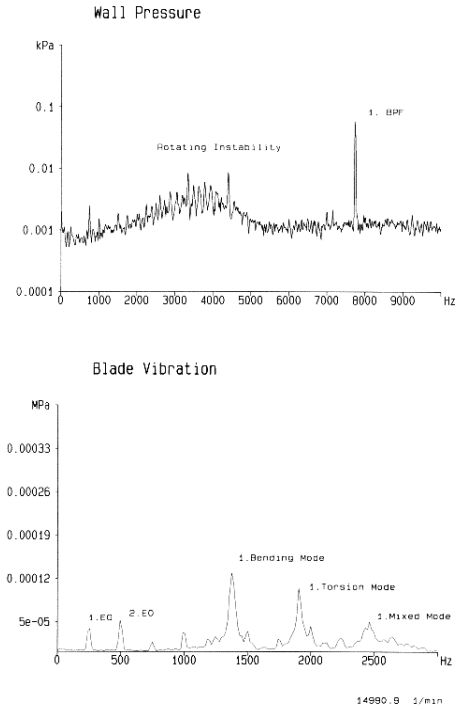

Figure 12: Comparison of wall pressure and blade vibration spectra, N=94 %.

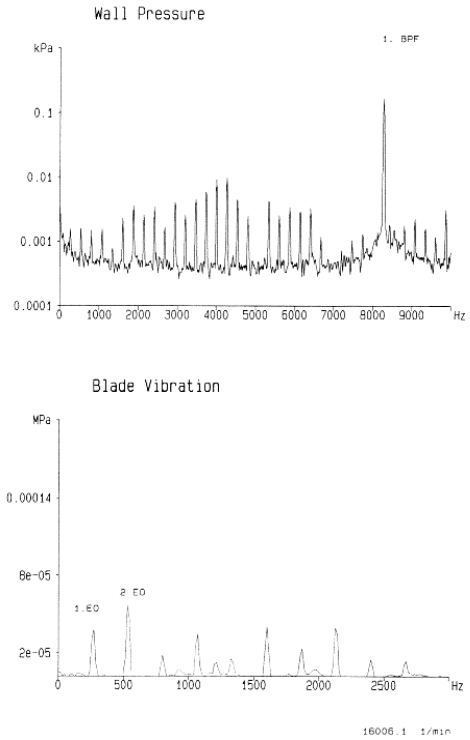

Figure 13: Comparison of wall pressure and blade vibration spectra, N=101 %.

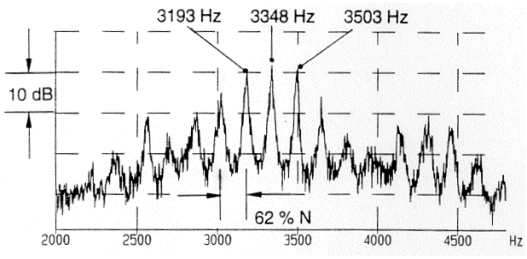

Figure 14: Power spectrum with an increased frequency resolution, N=94 %.

measured frequency pattern: A source frequency in a rotating frame, which is able to excite pressure waves with various nodal diameters, leads to a similar frequency behaviour in the fixed frame (Kameier and Neise, 1995 II).

The data analysed in this investigation show the same phenomenon of a rotating instability: A vortex shedding mechanism propagating relative to the rotor excites pressure waves with a certain frequency that can excitate rotor blades to high amplitudes.

5.3 Nodal Diameter and Source Frequency of Rotating Instability

To calculate the azimuthal mode number α according to equation (19) both the frequencies of the fixed and rotating frame are required. The frequencies of the fixed frame ω_{SM}^{F} can be taken from Fig. 14 whereas due to the lack of unsteady pressure instrumentation in the rotating frame only frequencies measured by strain gauges ω_{SM}^{R} can be employed. The 3rd and 4th columns of Table 1 give results for the positive and negative sign in equation (19). The source frequency

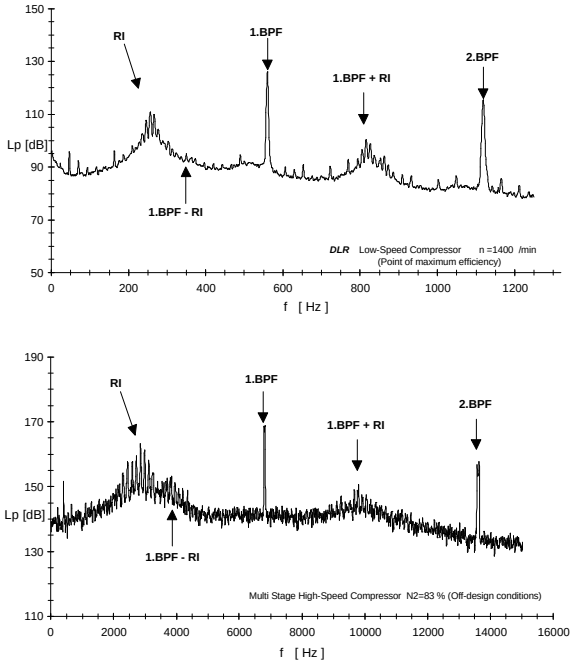

Figure 15: Pressure spectra at the casing wall, upstream the leading edge of the rotor; upper diagram: low-speed compressor (Kameier 1994); lower diagram: first stage of a multi-stage high-speed compressor of the present investigation.

ω_{SM}^{S} is being calculated by equation (12) considering that α and ω_{SM}^{F} might also be negative. Non-integer numbers of α are caused by inaccuracies of the frequency-data analysis, the lack of unsteady pressure instrumentation or non possible frequency combinations.

From a bladed disk analysis the mechanical nodal diameter was identified to be a 5th or 6th ND for the 1T family and a 7th or 8th ND for the 1F family. This

Table 1: Calculated aerodynamic nodal diameters α and source frequencies $\omega_{SM}^{S} > 0$, rotor speed $\Omega_R^F/2p = 249\ Hz$.

$\omega_{SM}^{F}/2\pi$ [Hz]	$\omega_{SM}^{R}/2\pi$ [Hz]	$\lvert\alpha\rvert = \frac{\lvert\omega_{SM}^{F}\rvert - \lvert\omega_{SM}^{R}\rvert}{\Omega_R^F}$	$\lvert\alpha\rvert = \frac{\lvert\omega_{SM}^{F}\rvert + \lvert\omega_{SM}^{R}\rvert}{\Omega_R^F}$	$\omega_{SM}^{S}/2\pi$ [Hz]				$\Omega_S^F/2\pi$ [Hz]
				$\lvert\alpha\rvert$ (-)		$\lvert\alpha\rvert$ (+)		
±3503	±1911	±6.4	±21.7	+2512	+4494	+133	+6873	+155
±3348	±1911	±5.8	±21.1	+2453	+4243	+74	+6622	+155
±3193	±1911	±5.1	±20.5	+2395	+3991	+16	+6370	+155
±3503	±1372	±8.6	±19.6	+2176	+4830	+468	+6538	+155
±3348	±1372	±7.9	±19.0	+2118	+4578	+410	+6286	+155
±3193	±1372	±7.3	±18.3	+2059	+4327	+351	+6035	+155

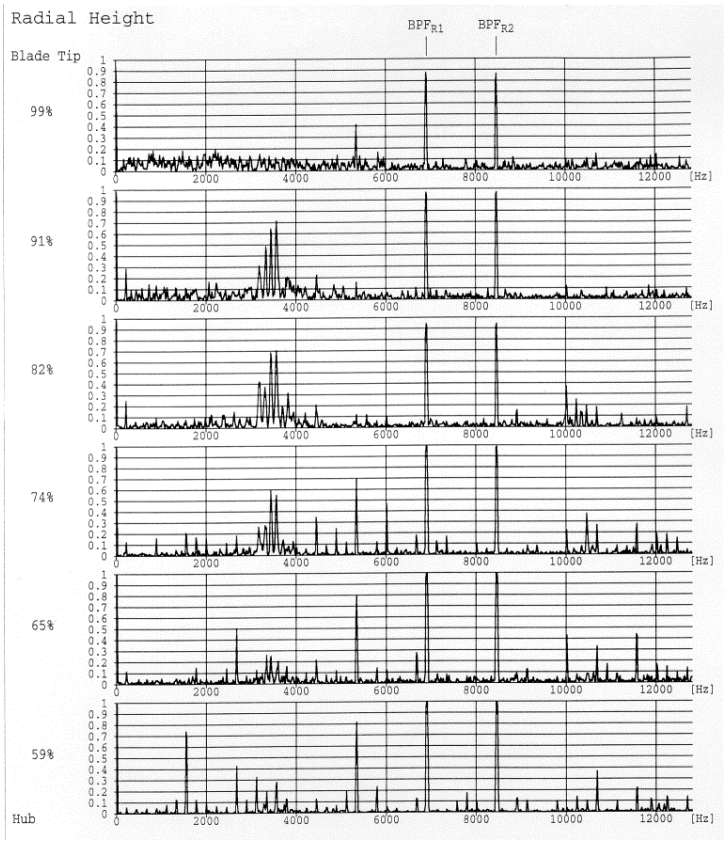

Figure 16: Coherence of pressure fluctuations at the casing wall (upstream leading edge of rotor 2) and velocity fluctuations (trailing edge of stator 1) for various blade heights, N=94%

would confirm the determination of the aerodynamic ND of the 3rd column in Table 1. The data of column 4 do not fit to the bladed disk eigenfrequencies.

The results show that a particular aerodynamic ND excites the same structural ND at a non-engine order resonance condition. The frequencies and the nodal diameters of the aerodynamical and mechanical waves are the same.

6. Measurement of the Radial Distribution of the Rotating Instability

To localise the radial extension of the rotating instability pattern hot-film measurements were carried out. At constant operating conditions the probe was radially moved downstream of the rotor close to the trailing edge. The position has been varied 40 % of the blade span from tip to hub.

Hot-film measurements near blade tips are subject to large measurement errors because close to the rotating blades both the magnitude and the angle of the mean velocity vary periodically by significant amounts. Therefore the results in Fig. 16 are displayed as spectra of the coherence function between the hot-film probe velocity fluctuations and the unsteady pressure probes in the casing wall

$$\gamma^2 = \frac{G_{21}(f) \cdot G_{21}^*(f)}{G_{11}(f) \cdot G_{22}(f)} \quad , \qquad (20)$$

where G_{11},G_{22} are the power spectra and G_{21} ,G_{21}^* conjugate complex cross-power spectra.

Apart from the blade passing frequency (BPF) of the 1st and 2nd stage, frequency peaks due to random fluctuations of the turbulent flow are quite large. In order not to lose the signal of the rotating instability effects these turbulent frequency spots were not averaged out.

Closest to the casing wall (upper spectrum, only half of the hot-film is in the flow) the velocity fluctuations are very noisy. This depends upon the installation of the hot-film probe in a hole where flow separation at the sharp edges occurs. At 91% blade height the rotating instability frequencies are clearly visible with high coherence levels. The levels are dying away with further movement of the hot-film probe to the centre. Eventually at 65% blade height the RI is no more detectable. The RI only occurs between the blade tip and the snubber. More studies are needed to investigate the impact of the snubber geometry on the RI phenomenon.

A further comparison of the total pressure distribution along the blade height indicates significant flow variations in the blade tip region at high pressure ratios especially at off-design conditions (94 % rotor speed). A continuous break down of the total pressure near the blade tip for an increasing pressure ratio is plotted in Fig. 17.

The unsteady measurements as well as the steady measurements of the total pressure distribution along the blade height confirm the supposition of the

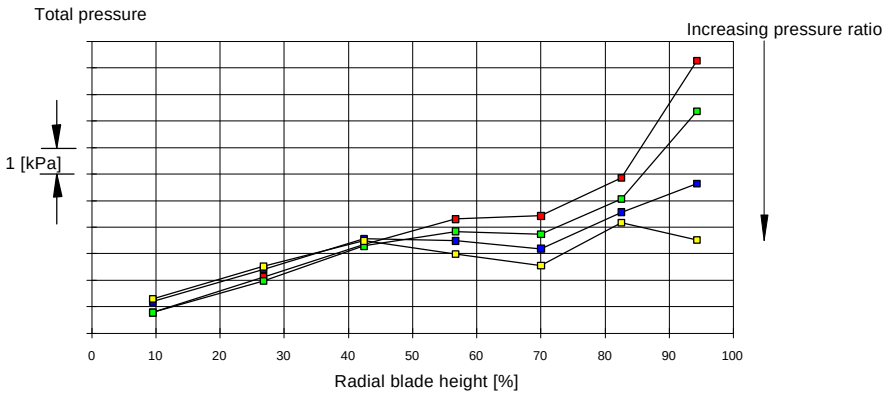

Figure 17: Total pressure distribution along blade height for different pressure ratios, N=94%, measured at stator 1.

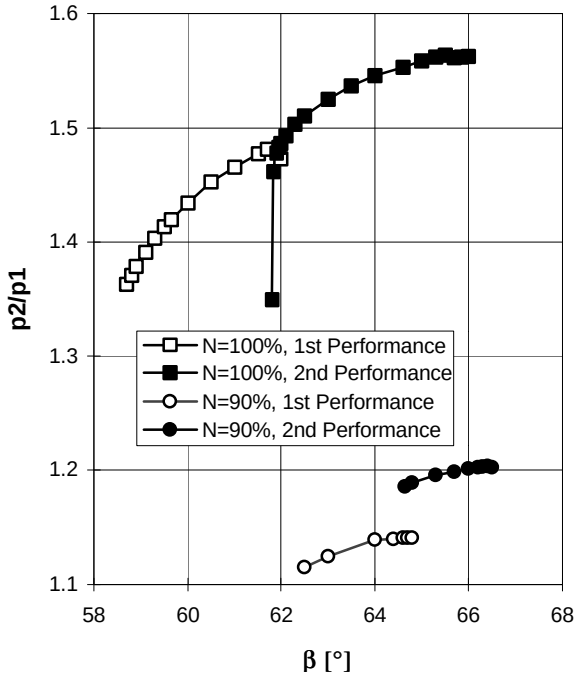

Figure 18: Profil loading for two different blade designs, numerical calculations. (Pressure ratio versus incidence)

rotating instability as a blade tip effect (part span stall).

7. Improvements of Aerodynamic Blade Loading

To reduce high aerodynamic blade loads in the tip region the first stage was modified. The aim was to move the operating conditions to greater incidence angles to achieve for the required mass flow rate the highest possible reserve against the operating conditions sensitive to instabilities. Fig. 18 shows for a cross-section in the blade tip area the new design allows more incidence and higher pressure ratio. Not only at design conditions but also at off-design conditions the flow stall begins at higher angles of attack.

8. Conclusions

An experimental investigation on a high pressure multi-stage compressor shows that for a certain operating condition high vibration levels on the first stage blades exist. The amplitudes are not in resonance with engine orders. Pressure fluctuations in the casing wall exhibit a characteristic pattern.

A theoretical model describes the effect: A sound source propagates relative to the rotor. It leads in its own frame of reference to an excitation of a series of sinusoidal pressure waves. The waves can be measured in the fixed and in the rotating system. The source has a particular frequency and is presumably caused by vortex shedding at off-design conditions. Resonance occurs if the bladed disk modes and the pressure waves have the same frequencies and the same nodal diameters. Because the source is moving relatively to the rotor the resonance happens at non-engine order conditions.

The frequency characteristic agrees well with results obtained on a low pressure fan experiment, where the propagation of the rotating source was investigated more in detail.

The rotating instability is similar to the rotating stall but the latter does not excite pressure fluctuations in its own frame of reference thus does not lead to the characteristic frequency range measured with pressure transducers.

Hot-film measurements have shown the radial dependency of this rotating instability phenomenon. In the investigated case it only occurs between blade tip and the snubber similar to a part span stall. Measurements of total pressure distribution along the blade span have also confirmed the effect.

9. Nomenclature

1F	1st flap (bending) mode of blade
1T	1st torsion mode of blade
N	Number of blades per stage
EO	Engine order
ND	Nodal diameter

BPF	Blade passing frequency
RI	Rotating instability
$p(\varphi,t)$	Pressure varying in circumferential direction φ and over time t
Ω_S	Angular velocity of rotating source
ω, A, Φ	Frequency, Amplitude and Phase angle of pressure wave
φ	Circumferential angle
ω_{SM}	Source-frequency
γ^2	Coherence function
G_{11},G_{12}	Power Spectrum, Cross Power Spectrum
Subscripts	
n	n-th Fourier-component
α	Numbers off circumferential nodal diameters of pressure wave
RS	Rotating stall
SM	Source mechanism
Superscripts	
F, S, R	Fixed, source and rotating frame of reference

10. References

Ewins, D.J., 1987: Structural Dynamic Characteristics of Bladed Assemblies, AGARD Manual on Aeroelasticity in Axial-Flow Turbomachines, AGARD-AG-298, Vol. 2.

Fletcher, N.H., Rossing, T.D., 1991: The Physics of Musical Instruments, Springer-Verlag, Berlin.

Fung, Y.C., 1955: An Introduction to the Theory of Aeroelasticity, John Wiley and Sons, New York.

Greitzer, E.M., 1980: Review - Axial Compressor Stall Phenomena, Journal of Fluids Engineering 102, pp. 134-151, June 1980.

Kameier, F., 1994: Experimentelle Untersuchung zur Entstehung und Minderung des Blattspitzen-Wirbellärms axialer Strömungsmaschinen, Fortschritt Berichte VDI Reihe 7, Nr. 243, Verein Deutscher Ingenieure, VDI Verlag GmbH, Düsseldorf, Germany (Doctoral Dissertation, Technische Universität Berlin).

Kameier, F.,Neise, W., 1995 I: Reduction of Tip Clearance Loss and Tip Clearance Noise in Axial-Flow Machines, AGARD PEP 85th Meeting on Loss Mechanisms and Unsteady Flows in Turbomachines, Derby, UK; 8-12 May.

Kameier, F., Neise, W., 1995 II: Rotating Blade Flow Instability as a Source of Noise in Axial Turbomachines, Proc. 1st CEAS/AIAA Aeroacoustic Conference München, June 12-15.

Parker, R., 1984: Acoustic Resonances and Blade Vibration in Axial Flow Compressors, Journal of Sound and Vibration, 92(4), pp. 529-539.

Parker, R., Stoneman, S.A.T., 1985: An Experimental Investigation of the Generation and Consequences of Acoustic Waves in an Axial Flow Compressor: Large Axial Spacing between Blade Rows, J. Sound and Vibration 99, pp. 169-182.

Sisto, F., 1987: Introduction and Overview, AGARD Manual on Aeroelasticity in Axial-Flow Turbomachines, AGARD-AG-298, Vol. 1.

Thomas, H.-J., 1956: Zur Frage der Gefährlichkeit von Paket- oder Einzelschwingungen bandagierter Turbinenschaufeln, Konstruktion 8 (1) pp.6-15.

Tyler, J.M., Sofrin, T.G., 1962: Axial Flow Compressor Noise Studies, SAE Transaction 70, pp. 309-332.